Supporting information (SI)

For

First Cage-Like Pentanuclear Co(II)-Silsesquioxane

by

A. N. Bilyachenko, A. I. Yalymov, M. M. Levitsky, A. A. Korlyukov, M. A. Es’kova, J. Long, J. Larionova, Y. Guari, L. S. Shul’pina, N. S. Ikonnikov, A. L. Trigub, Y. V. Zubavichus, I. E. Golub, E. S. Shubina, G. B. Shul’pin

Content

Experimental Section. S2
  Synthesis and characterization of **1** S2
  Structural description of **1** S3
  X-Ray study S3
  EXAFS S7
Proposed mechanism of cage of **1**’ assembly S9
Magnetic properties investigations S11
IR Measurements and computational details S13
Oxidation of alcohols and alkanes. Description of catalytic experiments S16
References S18

Experimental Section

Synthesis and characterization of 1.

“Spider Web”-like cobaltsodium phenylsilsesquioxane was prepared as previously reported[11] and dried in vacuum to remove coordinated solvates. $PhSi(OEt)_3$ was purchased from Acros organics and used as received. All solvents (Acros organics) were used without specific purification.

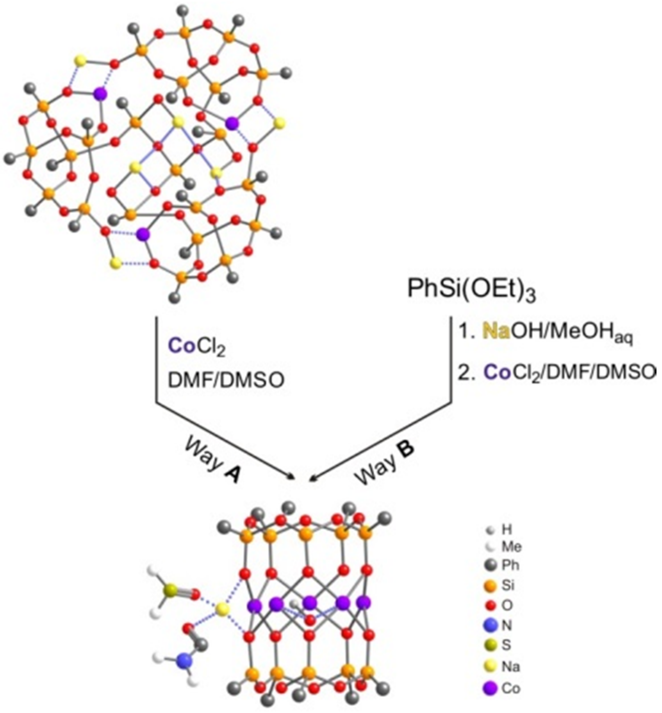

Figure S1. Schematic representation of the used approaches to the synthesis of **1**: from “Spider Web” compound (way A) or from phenyltriethoxysilane (way B).

Synthesis of $[(PhSiO_{1,5})_{10}(CoO)_5(NaOH)][DMF]_5[DMSO]_4$ 1.

Way A.

0.86 g (0.26 mmol) of cobaltsodiumphenylsilsesquioxane $[(PhSiO_{1.5})_{22}(CoO)_3(NaO_{0.5})_6]$, 35 ml of DMSO and 35 ml of DMF were placed in flask provided by magnetic stirrer and condenser. Resulted solution was heated to temperature of boiling; then 0.083 g (0.64 mmol) of $CoCl_2$ was added at once. Mixture was heated under reflux for 1 hour, then cooled to room temperature and filtered. To let slow evaporation of solvent the flask was stored at warm (~30 °C) place for several days. Just after the moment when liliac crystals began to grow, the flask was transferred to cool place and stored there for week. A few selected monocrystals were used for the X-ray diffraction analysis study (product’ composition was found to be $[(PhSiO_{1,5})_{10}(CoO)_5(NaOH)(DMF)_5(DMSO)_4]$): see details below). Yield (in calculation for vacuum dried sample $[(PhSiO_{1,5})_{10}(CoO)_5(NaOH)]$): 0.04 g (11%).

Synthesis of $[(PhSiO_{1,5})_{10}(CoO)_5(NaOH)][DMF]_5[DMSO]_4$ 1.
Way B.
3.6 g (0.015 mol) of $PhSi(OEt)_3$ in 75 ml of methanol and 0.45 g (0.025 mol) of water were stirred for 30 minutes. Then 0.60 g (0.015 mol) of NaOH was added and resulted mixture was heated to reflux for 2 hours. Afterwards solution was cooled down to room temperature and 0.81 g (0.0062 mol) of $CoCl_2$ was added at once. Solution was heated under reflux for 2 hours, then cooled down to room temperature and filtered. Volatiles were removed from filtrate in vacuum, resulted powder was recrystallized from DMF/DMSO mixture (35 ml/25 ml). Crystallization of mixture gave in 3 weeks liliac needles of crystal product. Several crystals were used for single crystal X-Ray investigation. The cell parameters were equal to those established for the compound obtained by means of way A. Samples for elemental analysis, EXAFS, magnetic measurements and catalytic tests were prepared by vacuum drying of crystal mass of the product without heating. Anal. Calcd. for $[(C_6H_5SiO_{1,5})_{10}(CoO)_5(NaOH)]$: Co, 17.27; Na, 1.35; Si, 16.46. Found: Co, 17.08; Na, 1.26; Si, 16.22. Yield: 29% (0.61 g).

Structural description of 1.

X-Ray study

X-ray data for **1** was measured with Bruker APEX DUO diffractometer. The structure was solved by charge flipping and refined using anisotropic approximation for atoms of metallasilsesquioxane moiety (Figure S2) and some coordinated molecules of DMF and DMSO. A part of DMF and DMSO molecules are disordered over two positions. The positions of hydrogen atoms were calculated from the geometrical point of view with fixed C-H bond length and equivalent displacement parameters. Analysis of Co…O0 distances and difference Fourier maps allowed us to locate the position of the hydrogen atom bonded to O0 atom. It was revealed that hydroxyl group participate in strong hydrogen bond with siloxanolate oxygen atoms O11 (O0…O11 and H0…O11 distances are 2.986(4) Å and 2.149(4) Å, the angle O0H0O11 is equal to 176.65(3)°). All calculations were carried out using SHELX[S1,S2] and OLEX2[S3] software. Experimental details and crystallographic information for **1** are summarized in Table S1.

Table S1. Crystal data and experimental details for **1**

Chemical formula	$C_{80.5}H_{103.5}Co_5N_{4.5}NaO_{29}S_{3.5}Si_{10}$
M_r	2308.92
Space group	*Pbca*
Temperature (K)	120
a, *b*, *c* (Å)	19.6119 (4), 27.1456 (5), 37.5545 (8)
V (Å^3)	19993.1 (7)
Z	8
Radiation type	Cu $K\alpha$ [$\lambda = 1.5418$Å]
μ (mm^{-1})	8.89
Crystal size (mm)	0.3 × 0.2 × 0.1

T_{min}, T_{max}	0.273, 0.753
No. of measured, independent and observed [$I > 2\sigma(I)$] reflections	74758, 17521, 10749
R_{int}	0.196
$2\theta_{\mathrm{max}}$ (°)	67.0
$R[F^2 > 2\sigma(F^2)]$, $wR(F^2)$, S	0.099, 0.266, 1.04
No. of reflections	17521
No. of parameters	1185
ρ_{max}, ρ_{min} (e Å^{-3})	1.45, -1.19

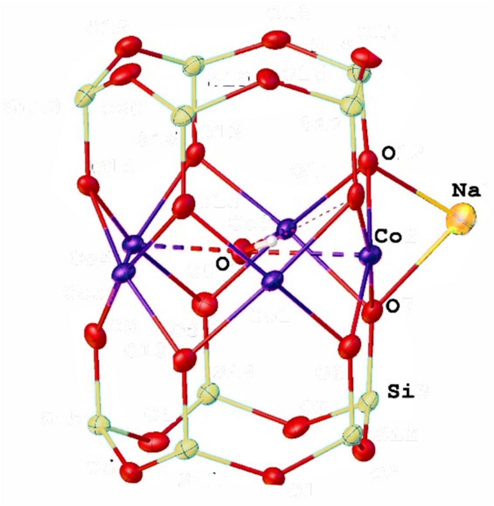

Figure S2. Molecular structure of **1**. Phenyl groups at silicon atoms and coordinated solvates are omitted in the sake of clarity.

One could observe that oxygen atoms exclusively participate in coordination environment of complex **1’** cobalt ions: four oxygen atoms of metallasiloxane fragments SiOCo, oxygen atom of encapsulated HO^- anion, and oxygen atom of solvate (DMF or, once, DMSO). Similarly, only oxygen atoms (of DMF, DMSO, and SiOCo fragment) coordinate sodium cation (Figure S3).

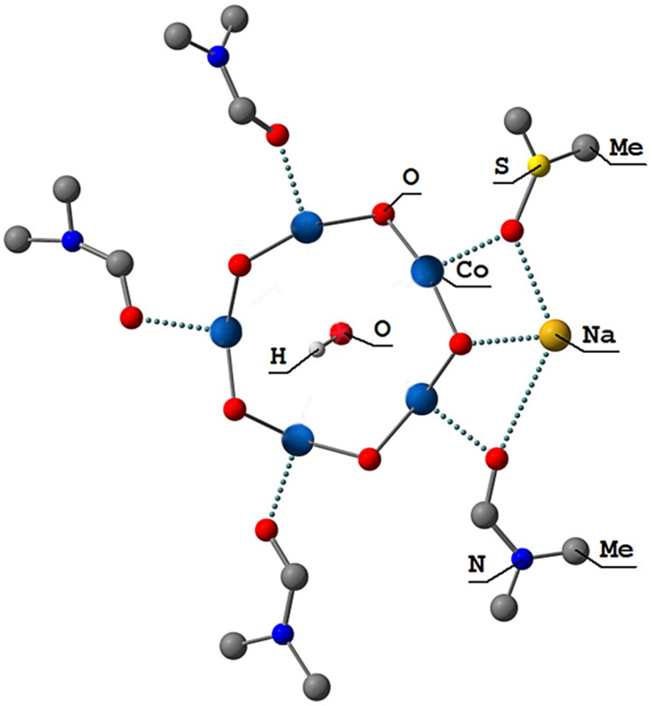

Figure S3. Features of cobalt and sodium ions coordination environment in **1.**

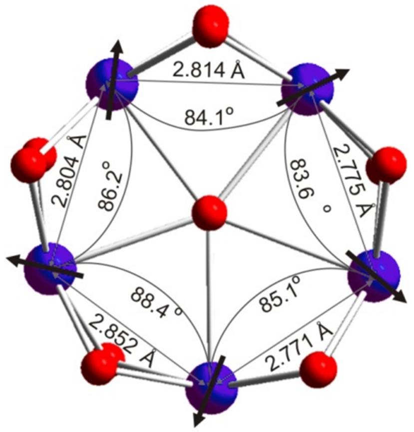

Figure S4. Topology of the Co(II) ions arrangement in **1**.

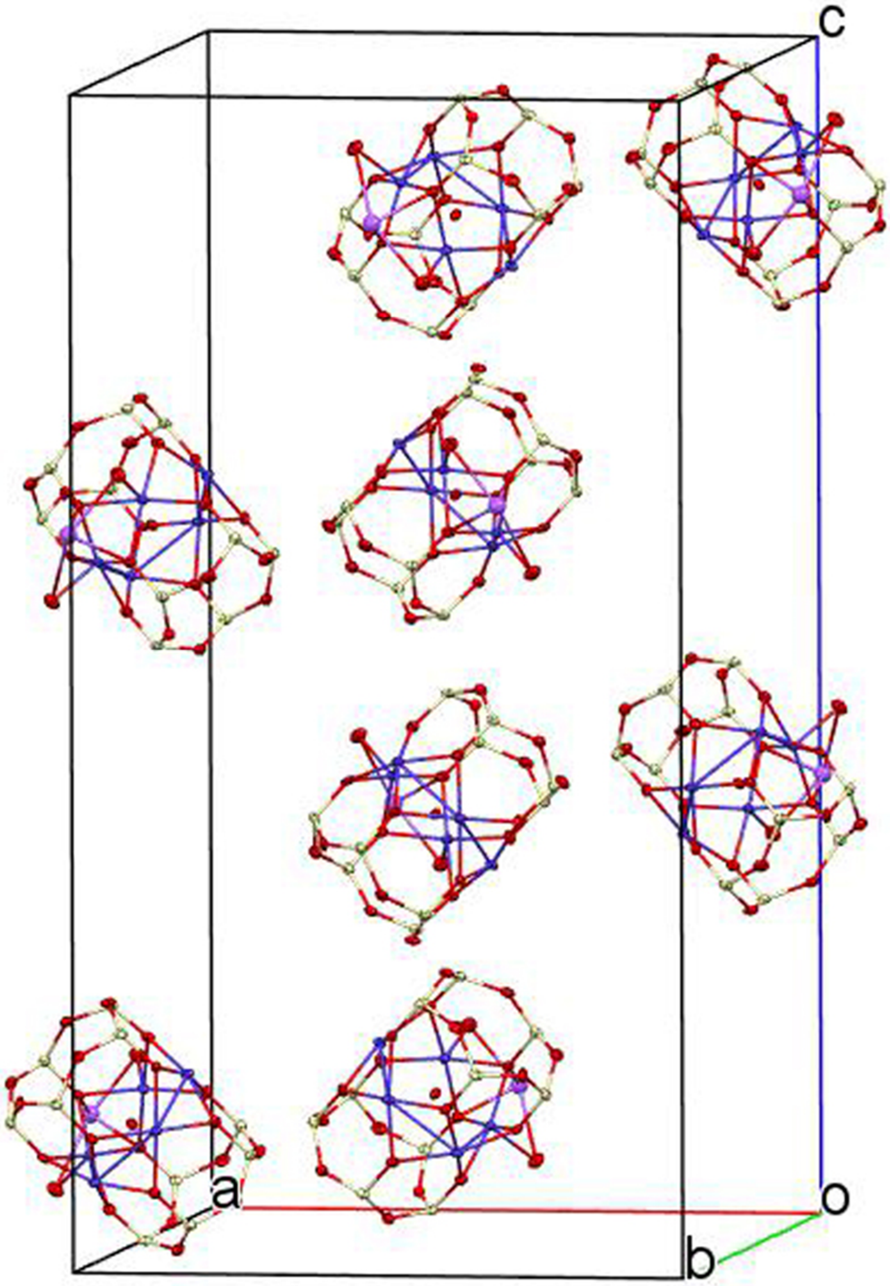

Figure S5. The view of crystallographic cell of **1**

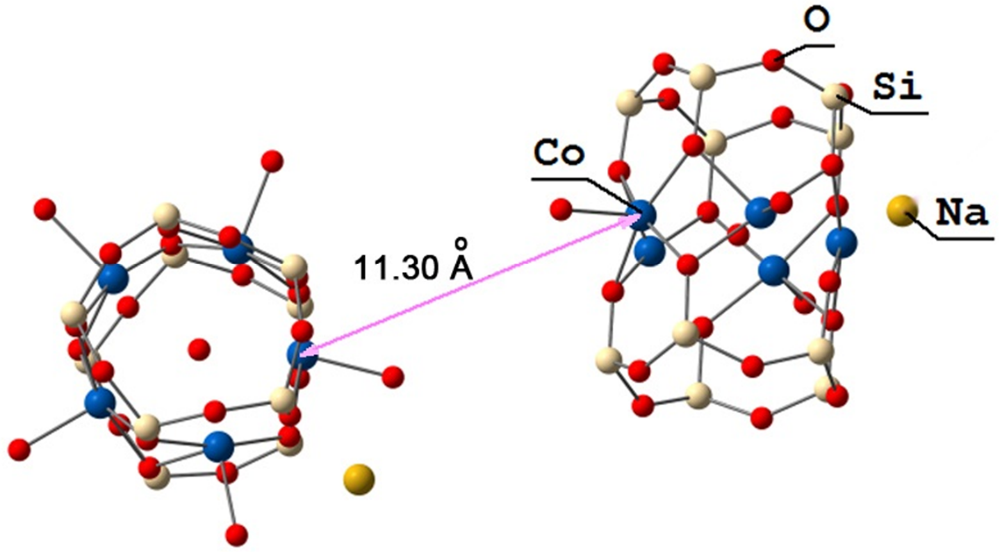

Figure S6. Crystal packing of **1.** The shortest intramolecular contact Co-Co is shown.

EXAFS

The Co K-edge X-ray spectra for sample in the solid state were collected at the beamline “Structural Materials Science”[S4] using the equipment of “Kurchatov Synchrotron Radiation Source” (Moscow,Russia). The storage ring with an electron beam energy of 2.5 GeV and a current of 80–100 mA was used as the source of radiation. All the spectra were collected in the transmission mode using a Si (111) channel-cut monochromator. The powder samples were spread over an adhesive Kapton tape that was folded into several layers to achieve an appropriate combination of total absorption and absorption edge jump. EXAFS data ($\chi_{exp}(k)$) were analyzed using the IFEFFIT data analysis package.[S5] EXAFS data reduction used standard procedures for the pre-edge subtraction and spline background removal. The radial pair distribution functions around the Co ions were obtained by the Fourier transformation (FT) of the k^2-weighted EXAFS functions $\chi_{exp}(k)$ over the ranges of photoelectron wave numbers k = 2.5–15.0 Å^{-1}. The structural parameters, including interatomic distances (R_i), coordination numbers (N_i) and Debye–Waller factors (σ^2), were found by the non-linear fit of theoretical spectra (Formula (1)) to experimental ones.

$$\chi(k) = S_0^2 \sum_{i=1}^{n} \frac{N_i F_i(k)}{R_i^2 k} e^{\frac{-2R_i}{\lambda(k)}} e^{-2\sigma_i^2 k^2} \sin\left(2kR_i + \varphi_i(k)\right) \tag{1}$$

The theoretical data were simulated using the photoelectron mean free path $\lambda(k)$, amplitude $F_i(k)$ and phase shift $\varphi_i(k)$ calculated *ab initio* using program FEFF6.[S6] For the refined interatomic distances (R_i) the statistical error is 0.01–0.02 Å for the first coordination sphere.

Parameters of local surrounding of cobalt atoms in sample **1** retrieved from Co K-edge EXAFS spectroscopy are fully consistent with crystallographic data (see Fig. S5). First shell of oxygen atoms for nonequivalent 5 cobalt atoms in crystal structure were fitted by two distances 2.05 Å (4 oxygen atoms) and 2.34 Å (2 oxygen atoms). Comparison of the radii for other atomic shells obtained by EXAFS and X-ray crystallography is presented in Table 2.

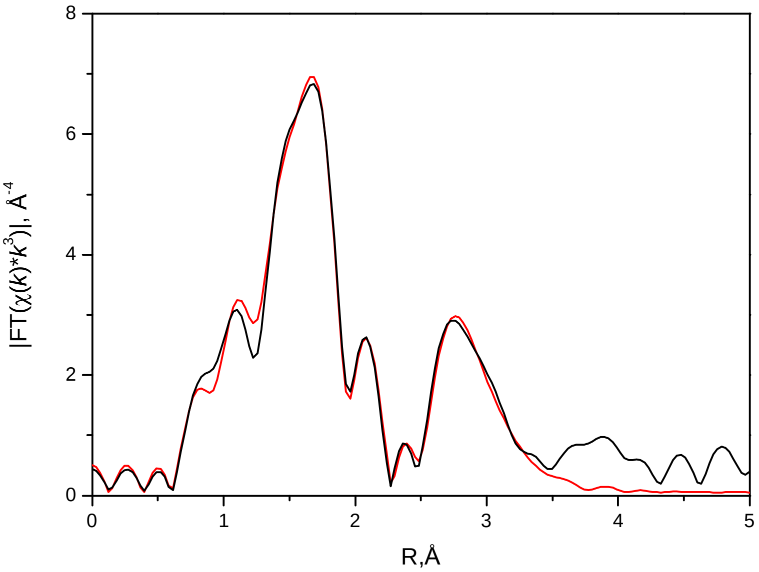

Figure S7. Fourier transform of Co K-edge EXAFS spectrum for **1**: experiment (black line) and best fit (red line)

Table S2. Radii of the nearest atomic shells obtained from EXAFS fitting and X-ray crystallography.

Co-X	R, Å EXAFS data	R, Å X-ray crystallography
Co-O	2.02	2.02-2.6
Co-O	2.13	2.07-2.16
Co-O	2.35	2.24-2.49
Co-Co	2.85	2.77-2.85
Co-Si	3.31	3.29-3.38

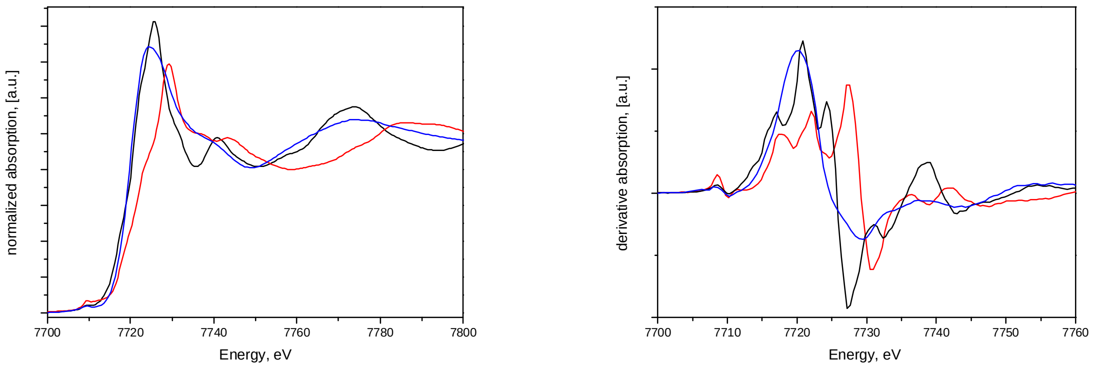

Figure S8. Comparison of normalized XANES spectra (left panel) and their derivatives (right panel) for CoO (black line), Co_2O_3 (red line) and **1**. Right panel: comparison of derivatives of normalized XANES spectra for CoO (black line), Co_2O_3 (red line) and **1**.

XANES spectra were used to investigate oxidation state of metal ion and symmetry of metal site. Fig. S8 (left panel) reports the XANES spectra of the sample and spectra for the standard compounds for cobalt ion in different oxidation states: Co^{+2} in CoO and Co^{+3} in Co_2O_3. All presented spectra have pre-edge feature at energy 7709 eV. To highlight the difference between the spectra it is useful to plot their derivatives, as shown on Figure S8 (right panel). From the comparison of presented XANES spectra and their derivatives, it could be concluded that compounds with Co(III) can be characterized by peak in derivative of the spectrum at ~7127 eV. As corresponding derivative of the investigated sample **1** exhibit no peak at ~7127 eV, it could be concluded that oxidation state of cobalt ions in **1** is +2 exclusively.

Proposed mechanism of cage of 1’ assembly

In our opinion, the structural arrangement of specific molecular architectures of cage-like metallasilsesquioxanes with prismatic structure may be explained as template synthesis. The cage may be formed through the coordination of metallasilsesquioxane fragments *in situ* around an organizing center. In present case of **1**, an encapsulated OH^- anion coordinates metallasilsesquioxane cycles while DMF and DMSO molecules, used for the synthesis/crystallization of **1**, let an effective solvation of external sodium ion (Figure S9).

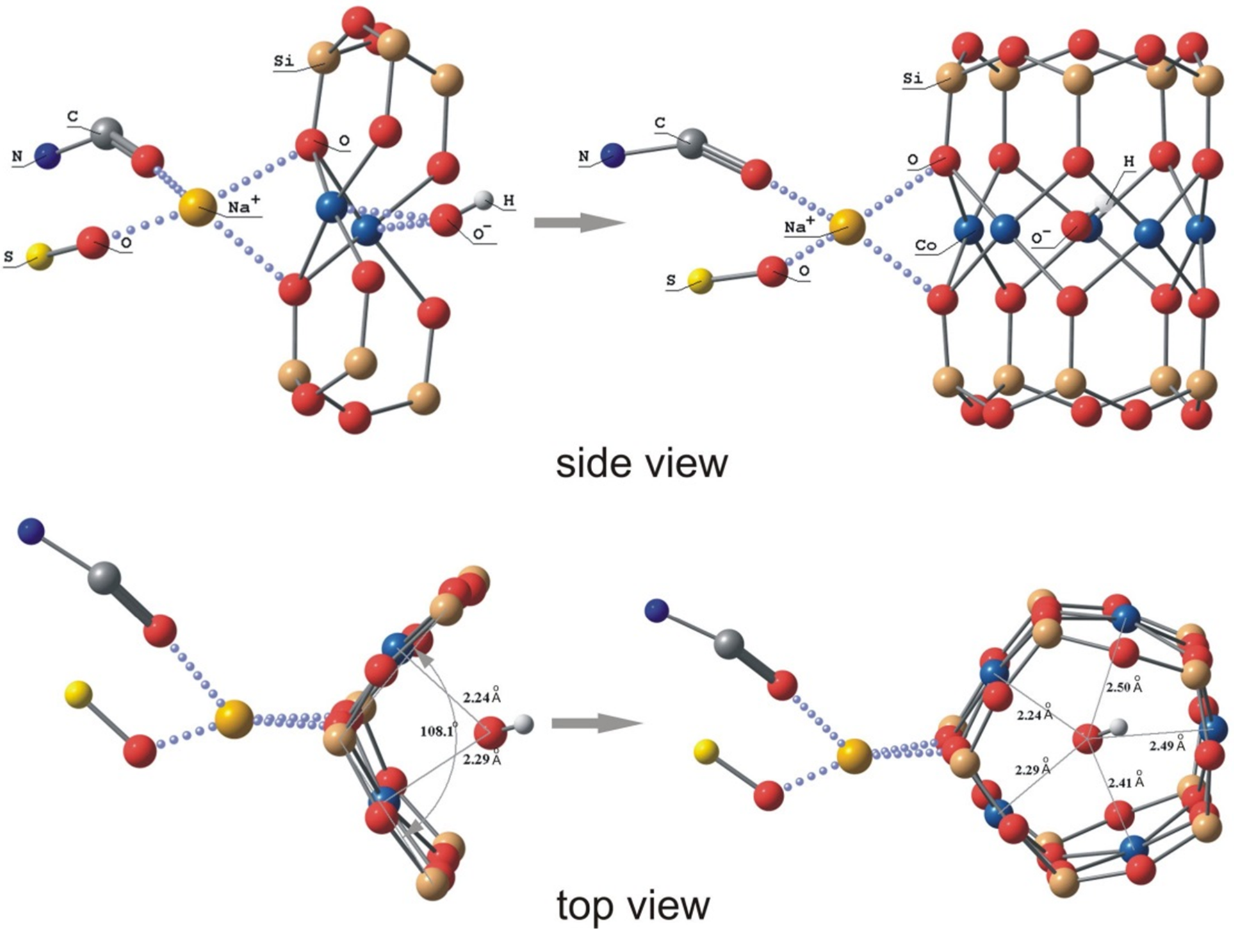

Figure S9. Suggested scheme of compound **1** formation. Coordination of metallasilsesquioxane fragments to OH^- and Na^+ centers in DMF/DMSO media.

Interesting that value of Si-Si-Si angle (formed by two metallasilsesquioxane cycles) is equal to 108.1°. This value almost coincides with the value known for the inner angle of a regular pentagon (108 °). Noteworthy, OH^- is located not exactly in the center of the formed cage, most probably, due to non-symmetricity of hydroxyl anion. The shortest distance between its oxygen and cobalt atoms is Co2…O0 (2.2491(10)) while the longest one is Co1…O0 (2.5010 (10) Å).

In turn, when organizing center is symmetrical, such as chloride anion, its localization an in the perfect center of cage is observed. In this case, the distances Co…Cl vary in the very narrow range (2.90-2.92 Å).[8b]

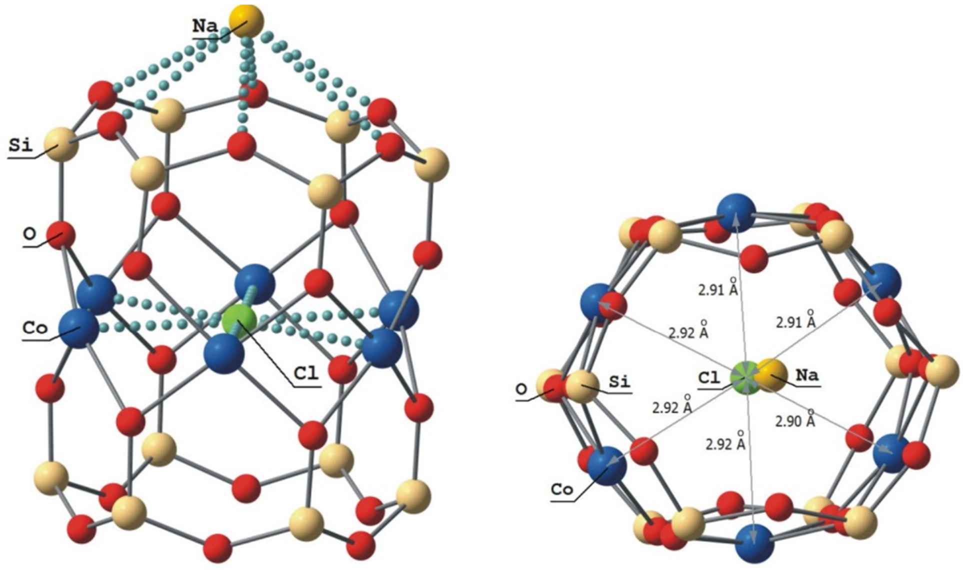

side view

top view

Figure S10. Simplified side and top views of hexanuclear Co(II) phenylsilsesquioxane from ref 4b.

Also, the pentanuclear cage **1** principally differs from a classical hexanuclear architecture[4b] by the type of sodium ion coordination to metallasilsesquioxane prism. While in the case of hexanuclear compound one could observe “crown ether”-like coordination of sodium cation to oxygen atoms of siloxane (Si-O-Si) cycle (Figure S11 left), cage **1** exhibits unusual “side coordination” of sodium cation to oxygen atoms of metallasiloxane (Si-O-Co) fragments (Figure S11 right). Probably, this type of coordination additionally favors before mentioned distortion of pentanuclear cage **1** framework (Co…Co distances vary in range 2.777 – 2.853). As oxygen atom of Si-O-Co fragment possesses higher basicity than one in Si-O-Si fragment, the Na-O distance in **1** is much shorter than in hexanuclear Co-phenylsilsesquioxane.[4b]

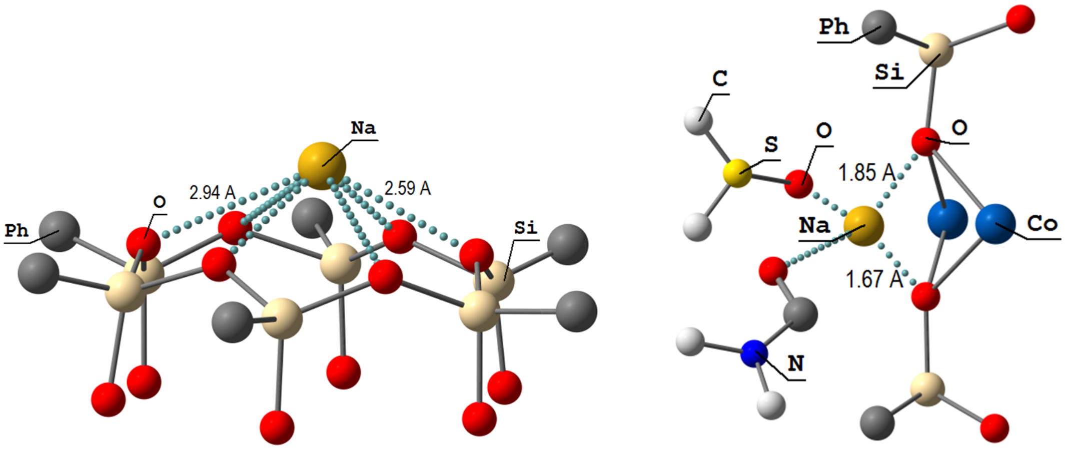

Figure S11. “Sodium to cage” coordination types in hexa[4b]- (left) and pentanuclear **1** (right) cobalt(II) phenylsilsesquioxanes.

Magnetic properties investigations

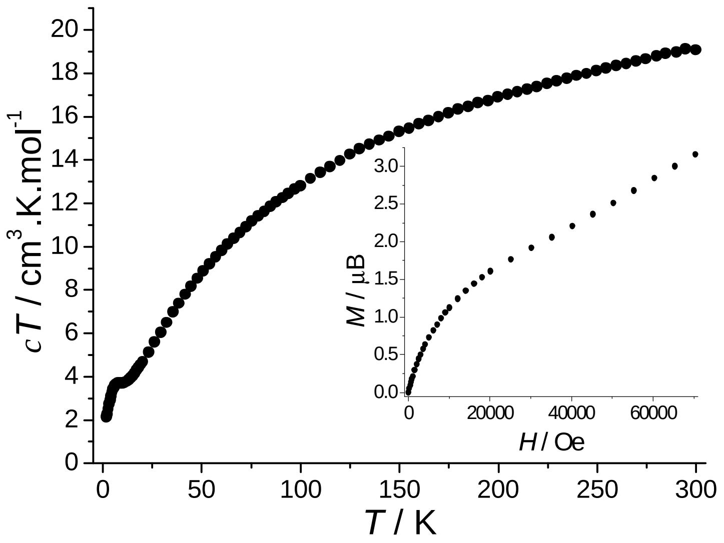

Figure S12. Temperature dependence of cT under a 1000 Oe DC field for **1**. Inset: Field dependence of the magnetisation at 1.8 K.

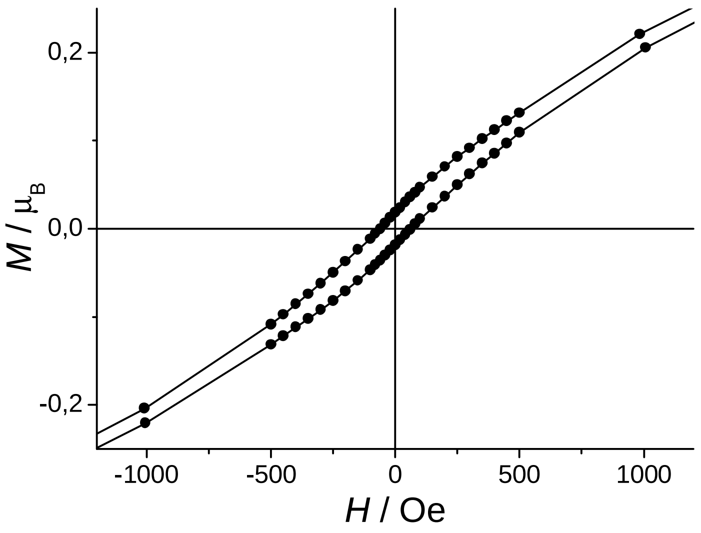

Figure S13. Hysteresis loop measured at 1.8 K.

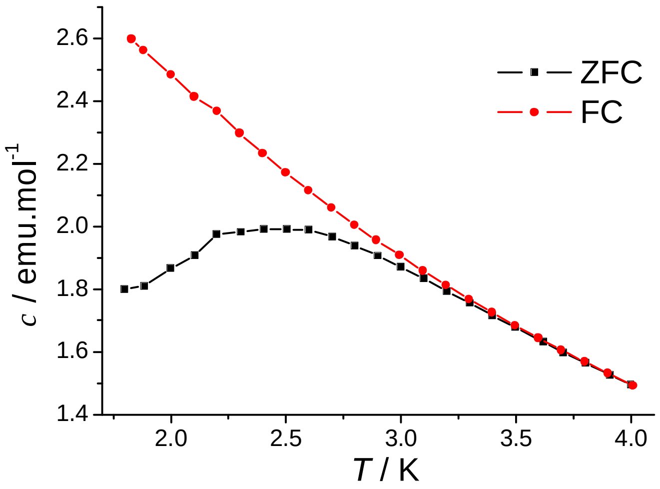

Figure S14. ZFC/FC curves measured under a 100 DC field.

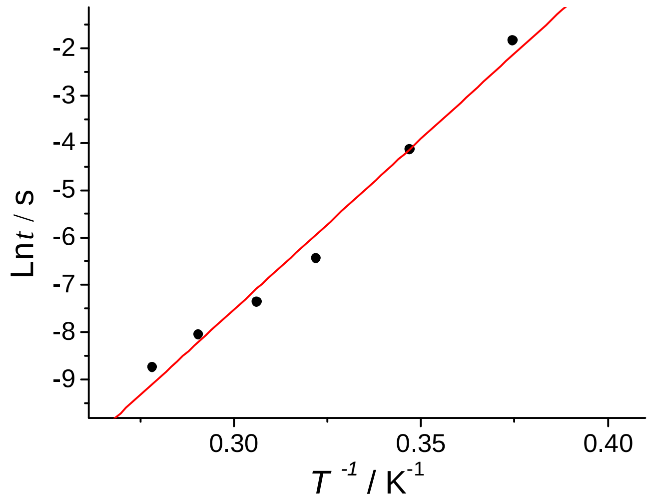

Figure S15. Temperature dependence of the relaxation time. The red solid line represents the Arrhenius law fit: the fitting of the blocking temperature was obtained from the*c''* maxima for different observation times *t =1/2pn* (with *n* being the frequency of the oscillating field).

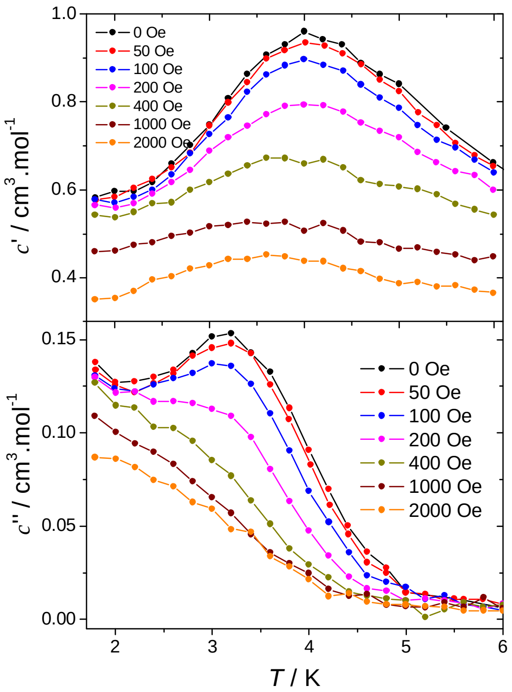

Figure S16. Temperature dependence of the ac susceptibilities (100 Hz) measured with various DC fields.

Details for the memory effect measurements. The sample was first rapidly cooled from 70 K down to 2.5 K in the absence of an external field, then a 100 Oe field was applied and a relaxation was measured for a time t_1 (black curve), yielding a magnetization for the molecules with the freezing temperature <2.5 K. The relaxation follows a logarithm curve, according to the energy distribution of the molecules. After t_1, the samples were quenched to 1.8 K in the presence of an external magnetic field (100 Oe) and the magnetization evolution was recorded during a time t_2 (red curve). A characteristic sharp jump in magnetization is observed due to the contribution of CLMS molecules with the blocking temperature <2.5 K, which reach their equilibrium state at 2.5 K and hence do not contribute to the magnetization. On the other hand, the molecules with the blocking temperature >2.5 K are out of equilibrium and relax extremely slowly at 1.8 K, leading to a constant curve during t_2. Thirdly, the temperature was returned back to 2.5 K, with the same magnetic field set at 100 Oe, and the magnetization was measured for a time t_3 (black curve). CLMSs with the blocking temperature <2.5 K and those flipped during time $t_1 + t_2$ come back to the new equilibrium state, which is same as that pertaining before quenching, and the relaxation during t_3 is the continuation of the time t_1.

IR Measurements. IR spectra of **1** were measured on FTIR Shimadzu IR Prestige-21 spectrometer in Nujol mull sandwiched between two KBr discs.

Computational Details. Full geometry optimization of **$Co_5Si_{10}C_{60}H_{50}O_{20}$** (the **1** with removed Na^+ and OH^- moieties as well as solvent shell) was provided with *Gaussian09*[S7] program package. The model was described by unrestricted open shell approach (UM06[S8] and UPBE0[S9] functional with spin-state-corrected s6-31G(d)[S10] basis set for Co atom and 6-31G for other atoms). Optimized structure shows very small differences from crystal structure (Table 3).

The optimized geometry reproduced quite well the silsesquioxane ligands (the difference between the calculated and experimentally observed for Si–O(Si) bonds and Si–μ^3-O$(Co)_2$ are less than 0.09 Å for UM06 (less than 0.13 Å for UPBE0) and 0.11 Å for UM06 (less than 0.15 Å for UPBE0) correspondingly. In turn, Co–μ^3-O(Si)(Co) bonds are slightly overestimated but not more than 0.15–0.16 Å for both methods. The quantum chemical calculation reveals: three Co atoms with Mulliken atomic spin density 1.00–1.04 for UM06 (1.01–1.06 for UPBE0) and two Co atoms with 2.72–2.73 for UM06 (2.49 for UPBE0), whereas total multiplicity of molecule was 10. Also, this calculation let us to compare positions of signals in IR spectra of **1** and optimized structures (Table S4, Fig. S18).

Table S3. Geometry parameters of crystal structure **1** and its optimized versions

Distances, Å	Crystal of **1**	**1_QM_UM06**	**1_QM_UPBE0**
Si–μ^2-O(Si)	1.581–1.651	1.674–1.711	1.707–1.725
Si–μ^3-O$(Co)_2$	1.589–1.606	1.699–1.710	1.731–1.751
Co–μ^3-O(Si)(Co)	2.017–2.163	1.869–2.024	1.880–1.999

Table S4. Experimental and the calculated values of IR-active bands

Vibration type	Experimental (Nujol mull)	**1_QM_UM06**	**1_QM_UPBE**
ν_{OH}^{bond}	3407	—	—
ν_{CH}	3074, 3049	3224–3210, 3174–3162	3161–3140
$Ph_{\text{-ring overtones}}$	1965, 1897, 1828, 1782	—	—
$\nu_{C–C}$	—	1666–1664	1606–1604
δ_{CH}	1428, 1418	1485–1483	1450–1448
$\nu_{C=C}$	—	1385–1382	1366–1364
δ_{CH}	1193	1204–1200	1210–1209
$\nu_{SiC(Ph)}$	1128	1168–1165	1127–1123
δ_{CH}	1091	1117–1114	1090
δ_{Ph}	1054–1005	1092–1026	1007–997
$\delta_{CH} + \nu_{SiO(Si)}$	1003–980	987–815	993–983
$\nu_{SiO(Co)(Co)}$	—	929–902, 888–815	916, 847–769
δ_{CH}	772	781–750	755–751

$\delta_{CC} + \delta_{SiO}$	738, 727	740–726	725–714
$\delta_{CH} + \delta_{CC} + \delta_{SiO}$	695	647–611	709–706, 608–595
$\nu_{CoO(Co)}$	—	583–581	539
δ_{CH}	497	494	506–476
δ_{SiO}	445, 440, 430	470–417	470–415
δ_{SiO}	—	402–380	397–342

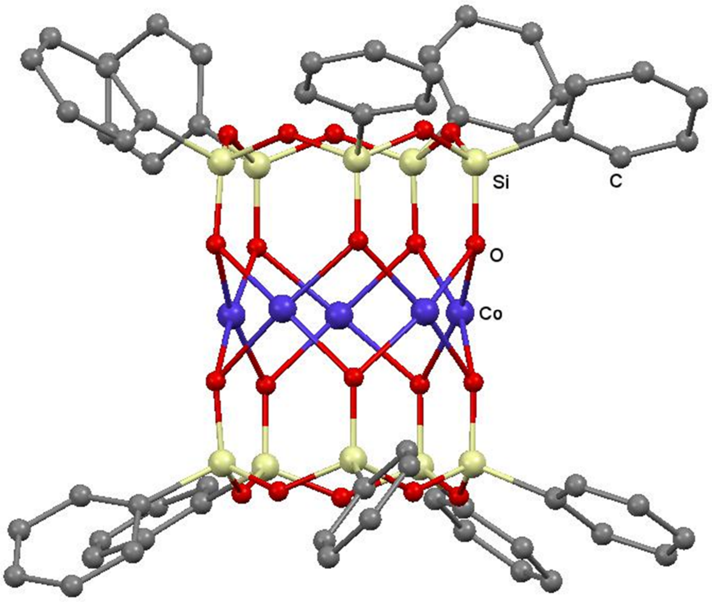

Figure S17. Optimized geometry of **1_QM (**DFT/UM06) (ball-and-stick model).

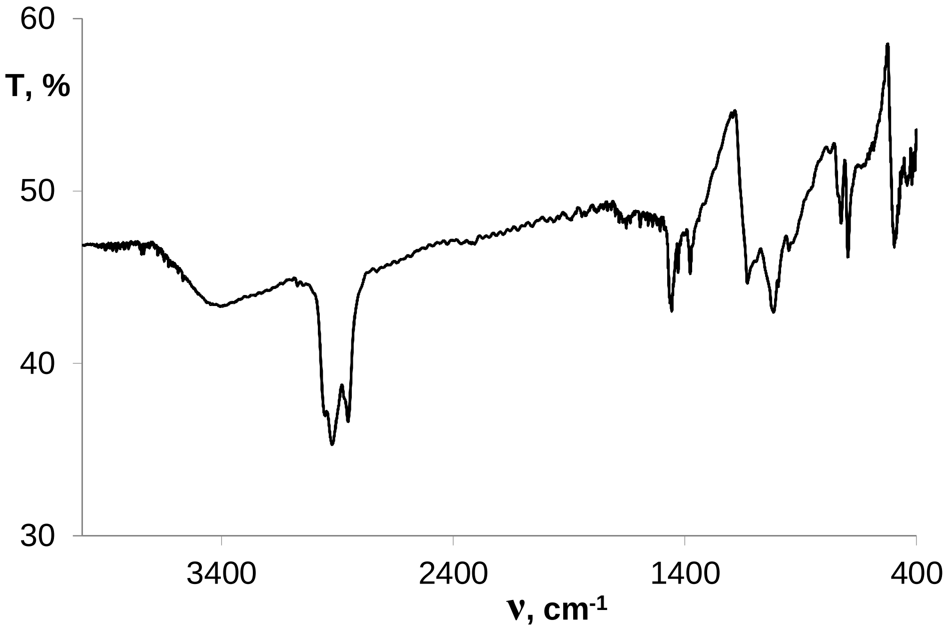

Figure S18. Spectrum of **1** in Nujol mull, sandwiched between two KBr discs.

Oxidation of alcohols and alkanes

Homogeneous (acetonitrile solution) oxidation of *n*-octane by *meta*-chloroperoxybenzoic acid (*m*-CPBA) gives isomers of *n*-octanone and *n*-octanol in 45 % total yield, after reduction with PPh_3.

Description of catalytic experiments

Catalysts **1** and Co_3Na_6-CLMS[7] were introduced into the reaction solution in acetonitrile containing a substrate and *m*-CPBA or TBHP. The reactions were typically carried out in air in thermostated Pyrex cylindrical vessels with vigorous stirring; total volume of the reaction solution was 2–5 mL. (Caution: the combination of air or molecular oxygen and peroxides with organic compounds at elevated temperatures may be explosive!) Samples of the reaction mixture were taken after certain time intervals, and concentrations of acetophenone were measured using ^{1}H NMR method (Bruker AMX-400 instrument, 400 MHz). Added to the sample acetone-d_6 was used as a component of the solvent (in addition to acetonitrile); 1,4-dinitrobenzene was a standard. The detection and quantification of the obtained products of the catalytic reactions were made by measuring the areas of peaks corresponding to methyl group from acetophenone (2.6 ppm). Products obtained from alkanes (see Table S5) were typically analyzed using GC method before and after adding PPh_3 to the reaction samples (chromatograph-3700, fused silica capillary column FFAP/OV-101 20/80 w/w, 30 m × 0.2 mm × 0.3 µm; helium as a carrier gas). Other conditions are given in the Table S5.

Table S5. Oxygenation of isomeric dimethylcyclohexanes with *m*-CPBA catalyzed by compound **1** [a]

Entry	Substrate	T (°C)	$[HNO_3]$ (M)	Time (min)	Reduction with PPh_3	*trans*-Dimethyl-alcohol (mM)	*cis*-Dimethyl-alcohol (mM)	Yield (%)	Ratio *trans*/*cis*
1[b]	*cis*-1,2-DMCH	40	0	120	yes	4	5.7	7	0.70
2[b]	*cis*-1,2-DMCH	50	0	30	yes	4	5	6	0.77
3[b]	*cis*-1,2-DMCH	50	0.05	30	yes	3	21	17	0.13
4[b]	*cis*-1,2-DMCH	40	0	300	yes	3	15	13	0.20
5	*cis*-1,2-DMCH	40	0	120	yes	40	38	56	1.0
6	*cis*-1,2-DMCH	40	0.05	5	yes	1.5	31	23	0.05
7				15	no	3	55	41	0.05
8					yes	3	55	41	0.05
9				30	no	3	79	59	0.04
10					yes	4	83	62	0.05
11				120	no	3	76	56	0.04
12					yes	4	76	57	0.05
13				300	no	4	76	57	0.05
14					yes	4	75	56	0.05
15[c]	*cis*-1,2-DMCH	40	0.05	30	no	12	78	64	0.15
16[c]					yes	12	68	57	0.18
17[c]				120	yes	12	71	59	0.17
18	*trans*-1,2-DMCH	40	0.05	15	no	38	3	30	13
19					yes	33	2	25	16
20				120	no	44	3	34	15
21					yes	42	3	32	14
22	*cis*-1,4-DMCH	40	0.05	15	yes	19	59	56	0.32
23				120	yes	17	54	51	0.31
24	*trans*-1,4-DMCH	40	0.05	15	yes	33	2	25	16
25				120	yes	31	2	24	16

[a] Reactions were performed in MeCN (total volume 2.5 mL). Concentrations: $[\text{Substrate}]_0 = 0.14$ M, $[m\text{-CPBA}]_0 = 0.26$ M, $[\text{catalyst } \mathbf{1}]_0 = 5 \times 10^{-4}$ M. [b] In the absence of catalyst **1**. [c] Trinuclear cobalt catalyst **2** (see Ref. 4) was used instead of catalyst **1**.

References:

S1 Sheldrick, G. M. A Short History of SHELX. Acta Cryst. 2008, A64 (1), 112–122

S2 Sheldrick, G. M. Crystal Structure Refinement with SHELXL. Acta Cryst 2015, C71 (1), 3–8

S3 Dolomanov, O. V.; Bourhis, L. J.; Gildea, R. J.; Howard, J. A. K.; Puschmann, H. OLEX2: A Complete Structure Solution, Refinement and Analysis Program. J. Appl. Cryst. 2009, 42 (2), 339–341

S4 A.A. Chernyshov, A.A. Veligzhanin, Y.V. Zubavichus, Nucl. Instr. Meth. Phys. Res.A 603 (2009) 95-98

S5 M. Newville, J. Synchrotron Rad. (2001) 96

S6 S.I. Zabinski, J.J. Rehr, A. Ankudinov, R.C. Alber, Phys. Rev. B52 (1995) 2995

S7 Frisch, M. J.; Trucks, G. W.; Schlegel, H. B.; Scuseria, G. E.; Robb, M. A.; Cheeseman, J. R.; Scalmani, G.; Barone, V.; Mennucci, B.; Petersson, G. A.; Nakatsuji, H.; Caricato, M.; Li, X.; Hratchian, H. P.; Izmaylov, A. F.; Bloino, J.; Zheng, G.; Sonnenberg, J. L.; Hada, M.; Ehara, M.; Toyota, K.; Fukuda, R.; Hasegawa, J.; Ishida, M.; Nakajima, T.; Honda, Y.; Kitao, O.; Nakai, H.; Vreven, T.; Montgomery, J. A.; Peralta, J. E.; Ogliaro, F.; Bearpark, M.; Heyd, J. J.; Brothers, E.; Kudin, K. N.; Staroverov, V. N.; Kobayashi, R.; Normand, J.; Raghavachari, K.; Rendell, A.; Burant, J. C.; Iyengar, S. S.; Tomasi, J.; Cossi, M.; Rega, N.; Millam, J. M.; Klene, M.; Knox, J. E.; Cross, J. B.; Bakken, V.; Adamo, C.; Jaramillo, J.; Gomperts, R.; Stratmann, R. E.; Yazyev, O.; Austin, A. J.; Cammi, R.; Pomelli, C.; Ochterski, J. W.; Martin, R. L.; Morokuma, K.; Zakrzewski, V. G.; Voth, G. A.; Salvador, P.; Dannenberg, J. J.; Dapprich, S.; Daniels, A. D.; Farkas; Foresman, J. B.; Ortiz, J. V.; Cioslowski, J.; Fox, D. J., Gaussian 09, Revision C.01, Gaussian, Inc.,. In Wallingford CT, 2009.

S8 Zhao, Y.; Truhlar, D., Theor. Chim. Acta 2008, 120, 215-241.

S9 Perdew, J. P.; Burke, K.; Ernzerhof, M., Phys. Rev. Lett. 1996, 77, 3865-3868.

S10 Swart, M.; Güell, M.; Luis, J. M.; Solà, M., J. Phys. Chem. A 2010, 114, 7191-7197